SCIENTIFIC REPORTS

OPEN

SUBJECT AREAS:
CATALYST SYNTHESIS
CHEMICAL ENGINEERING

Received
17 July 2013

Accepted
20 September 2013

Published
9 October 2013

Correspondence and requests for materials should be addressed to J.-I.P. (parkjoo9@asem.kyushu-u.ac.jp) or Y.-G.S. (shulyg@yonsei.ac.kr)

* These authors contributed equally to this work.

Hollow Fibers Networked with Perovskite Nanoparticles for H_2 Production from Heavy Oil

Yukwon Jeon[1]*, Dae-Hwan Park[1,3]*, Joo-Il Park[2], Seong-Ho Yoon[2], Isao Mochida[2], Jin-Ho Choy[3] & Yong-Gun Shul[1]

[1]Department of Chemical and Biomolecular Engineering, Yonsei University, Yonsei-ro 50, Seodaemun-gu, Seoul 120-749, Korea, [2]Institute for Materials Chemistry and Engineering, Kyushu University, 6-1 Kasuga-koen, Kasugasi, Fukuoka 816-8580, Japan, [3]Center for Intelligent NanoBio Materials (CINBM), Department of Chemistry and Nano Science and Department of Bioinspired Science, Ewha Womans University, Seoul 120-750, South Korea.

Design of catalytic materials has been highlighted to build ultraclean use of heavy oil including liquid-to-gas technology to directly convert heavy hydrocarbons into H_2–rich gas fuels. If the H_2 is produced from such heavy oil through high-active and durable catalysts in reforming process that is being constructed in hydrogen infrastructure, it will be addressed into renewable energy systems. Herein, the three different hollow fiber catalysts networked with perovskite nanoparticles, $LaCr_{0.8}Ru_{0.2}O_3$, $LaCr_{0.8}Ru_{0.1}Ni_{0.1}O_3$, and $LaCr_{0.8}Ni_{0.2}O_3$ were prepared by using activated carbon fiber as a sacrificial template for H_2 production from heavy gas oil reforming. The most important findings were arrived at: (i) catalysts had hollow fibrous architectures with well-crystallized structures, (ii) hollow fibers had a high specific surface area with a particle size of ≈50 nm, and (iii) the Ru substituted ones showed high efficiency for H_2 production with substantial durability under high concentrations of S, N, and aromatic compounds.

An oil jackpot of up to 233 billion barrels has been discovered in Australia, the new Saudi Arabia, which is foreseeable to extend the practical use of petroleum to about 200 years from 40 years at today's oil consumption rate. With a rising concern for gradual fossil fuel exhaustion, an efficient use of such oil resources is faced to an imperative emerging issue towards hydrogen economy based on sustainable energy generation. Hydrogen-based fuel cells that can be used for both automotive and stationary applications require a stable source of H_2 produced with a high efficiency reforming process[1–4]. The use of pure H_2 as a fuel in automotive and residential applications faces the costly process of distillation and/or hydro-treatment of naphtha. One approach to overcoming such limitations is the use of direct reforming of gas oil (heavy hydrocarbons) over a heteroatom-resistant catalyst. This process would be profitable because of the infrastructural reasons and the economical price of starting feeds compared with naphtha hydrocarbon fuels[5,6]. Gas oils contain various hetero-atoms such as S and N, including those present in aromatic species, depending on the mining location. In particular, the high content of S molecules, especially refractory species such as alkyl substituted dibenzothiophene (x,y-DBT) in gas oil, compared to other liquid hydrocarbons like logistic fuel or commercial diesel, is a crucial factor to consider when trying to achieve value-added products[7–9]. This needs to be considered when designing the catalyst since such hetero-atoms can be deactivating[10–12]. Nevertheless, in order to be commercially viable, gas oil appears to be an attractive feed for reforming because of its similar molecular structure to conventional diesel and/or liquid hydrocarbons, apart from its higher S content. There are no reports on reforming using gas oil, which is likely due to the rapid deactivation of conventional catalysts by large amounts of S species during the reaction. Hence, the development of a highly active and stable reforming catalyst under high S and N conditions would be desirable in order to apply the reforming process to gas oil.

Perovskite materials with a formula of ABO_3, where the A cation is 12-fold coordinated and the B cation is 6-fold coordinated with the oxygen, have been interested in various applications such as catalysis, energy, environment and bioscience applications[13–18]. Recently, noble methods for preparation of perovskite with unique architecture and morphology have emerged in the form of porous, scaffold, and egg-shell skeleton due to their high geometric surface area with large cavities, light weight and flexibility for mass and heat transfer[19–23]. To achieve such perovskite materials, templates such as polymer and biomolecules have been explored to manipulate their structure, crystallinity, size and shape, which cannot be obtained by the conventional methods[24–27]. In such a

way, crystal growth and configuration of the perovskites can be controlled since templates act as a dispersion agent and steric stabilizer for the deposition of metal precursors on them. Perovskite catalysts composed of highly reactive metal oxides have been highlighted as an alternative to conventional noble metal catalysts for the reforming of hydrocarbons. These catalyst materials have a number of advantages, including stability at high temperatures, in redox environments, and in the presence of H_2-rich gases. Moreover, perovskites are known to be significantly resistant to deactivation since their chemical binding energy for S is very low[28,29]. In particular, the perovskite of $LaCrO_3$ is stable because it is well known to strongly prefer six-fold coordination and the Cr in the B-site can be partially substituted for Ru, Ni, or Fe etc, providing catalytic activity that is extremely promising for the reforming of heavy hydrocarbons like gas oils[28–31].

In this work, a hollow fibrous perovskite structure composed of nanoparticles network incorporated with Ru and Ni was prepared through a novel process by employing activated carbon fiber (ACF) as a sacrificial template. The catalytic activity of the prepared hollow perovskite fibers in the production of H_2 from gas oils with different S and N contents through autothermal reforming (ATR) was investigated for the first time.

Results

Hollow fiber architechtures with a multi mixed perovskite nanoparticles are designed for an efficient mass tranfer including short diffusion and high contact time with the reactants in the autothermal reforming system[32]. The Synthesis procedure of the perovskite hollow fiber was shown in the Fig. 1A. The acid-treated ACF template was immersed in a solution of stoichiometric La^{III}, Cr^{III}, Ni^{II} and Ru^{III} ions, resulting in ionic binding of the metal cations to the negatively charged surface of the ACF. The hollow fiber composed of a perovskite nanoparticle network could then be successfully formed by mild heat treatment of the each $La^{III}Cr^{III}_{0.8}Ru^{III}_{0.2}$/ACF, $La^{III}Cr^{III}_{0.8}Ru^{III}_{0.1}Ni^{II}_{0.1}$/ACF, and $La^{III}Cr^{III}_{0.8}Ni^{II}_{0.2}$/ACF composite at 1027 K under air flow to remove the C content via combustion. For the formation of crystalline networks, ACF promotes the nucleation of nanoparticles at mild temperatures by an in-situ CO generation from the oxidative exothermic decomposition of ACF at the interface with metal cations[25–27].

According to the powder X-ray diffraction (XRD) patterns shown in Fig. 1B, all perovskites exibit major diffraction peaks in similar angle regions, corresponding to the (hkl) indices (112), (022), (220), (222), (312), and (040). These are exactly the same as those from the orthorhombic structure of $LaCrO_3$ perovskite with space group Pbnm, which matches the set of peaks reported in the powder diffraction file (PDF) no. 00-024-1016[31,33]. The stoichiometric chemical composition for all the perovskites was found to be by ICP-AES analysis (Table S1). From the magnified image showing the (112) reflection, substitution of Ru^{III} and Ni^{II} into $LaCrO_3$ can be seen to have caused a peak displacement to a lower angle when the substitution level is fixed with the ratio of 0.2 at the B-site. This implies an increase in the *d*-value (basal spacing) from 2.739 Å ($LaCrO_3$) to 2.764 Å ($LaCr_{0.8}Ru_{0.2}O_3$), 2.761 Å ($LaCr_{0.8}Ru_{0.1}Ni_{0.1}O_3$), and 2.756 Å ($LaCr_{0.8}Ni_{0.2}O_3$), in addition to the cell parameters and cell volume. As can be seen in Table S2, there were slight increases for the $LaCr_{0.8}Ru_{0.2}O_3$ in b-axis and c-axis cell parameters from 5.478 Å to 5.526 Å ($\Delta b = 0.048$ Å) and from 7.736 Å to 7.835 Å ($\Delta c = 0.099$ Å), respectively. These differences can be attributed to the different crystal ionic radii by partial substitution of Cr^{III} ion with Ru^{III} ion in the B site[34]. When the Ru^{III} metal ion is more substituted in perovskite lattices, their *d*-values were further shifted rather than the only Ni^{III}-substituted one.

The SEM images in Fig. 2A show the perovskite with a relatively 1D hollow fibrous structures for different chemical compositions with outer and inner fiber diameters in the ranges of 4.5–6.4 μm and 4.1–6.0 μm, respectively, and a length/diameter ratio of around 50, which corresponded well to the ACF template structure.

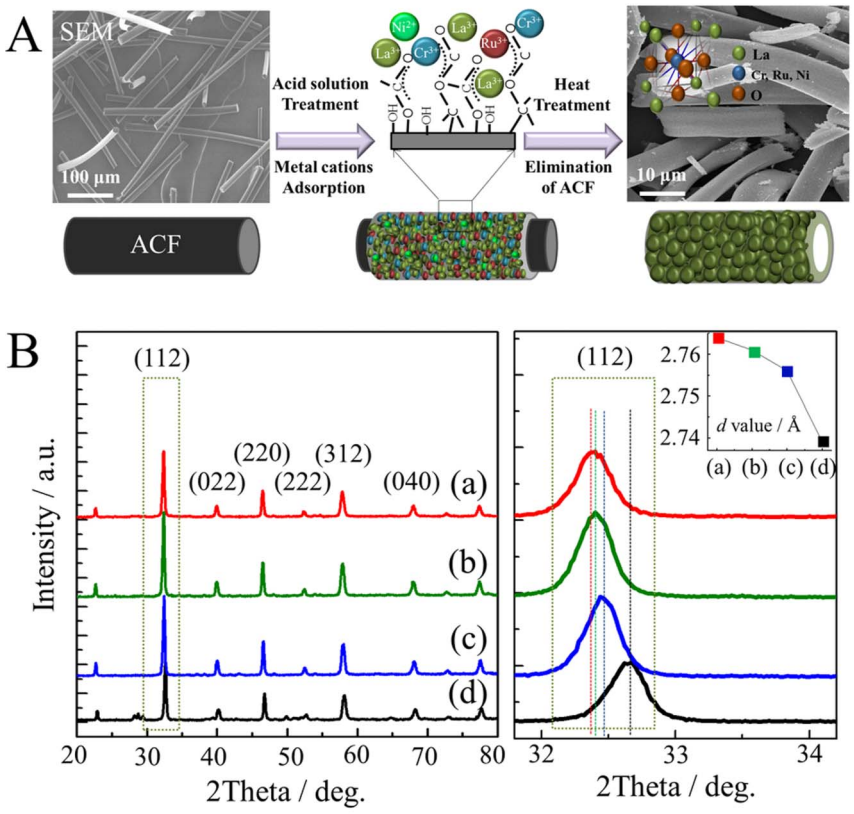

Figure 1 | A. Schematic diagram of the formation of hollow fibrous perovskite B. XRD patterns of the hollow fibers: (a) $LaCr_{0.8}Ru_{0.2}O_3$, (b) $LaCr_{0.8}Ru_{0.1}Ni_{0.1}O_3$, (c) $LaCr_{0.8}Ni_{0.2}O_3$, and (d) $LaCrO_3$.

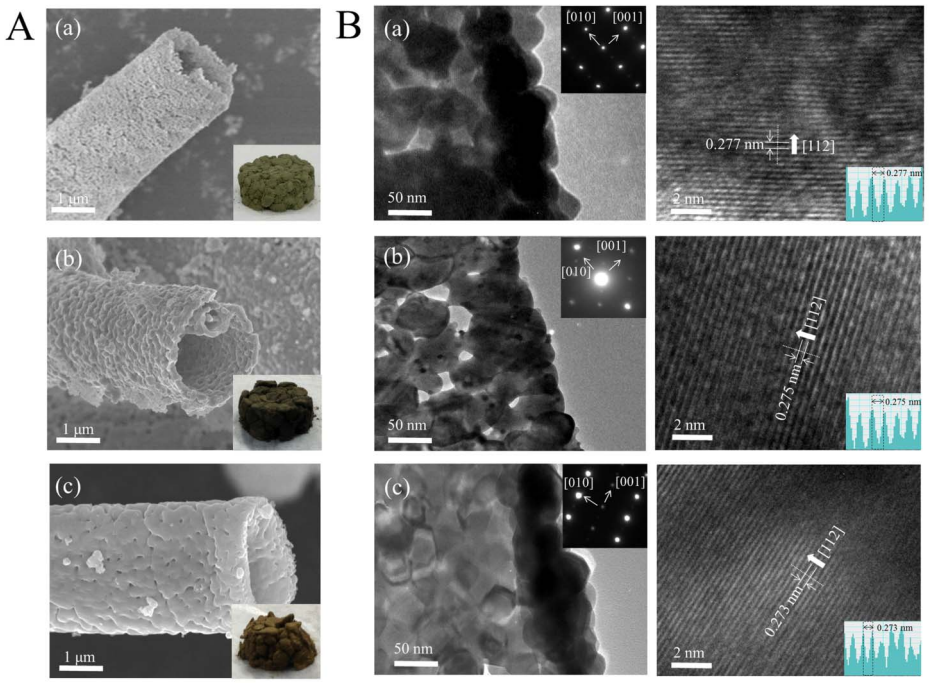

Figure 2 | A. SEM images (inset: photograph) and B. HR-TEM images (inset: SAED pattern and height profile) of the hollow fibers: (a) $LaCr_{0.8}Ru_{0.2}O_3$, (b) $LaCr_{0.8}Ru_{0.1}Ni_{0.1}O_3$, and (c) $LaCr_{0.8}Ni_{0.2}O_3$.

Furthermore, in the photograph, different colors of the perovskite hollow fibers were clearly obtained from the spesific incorporation metals.

As illustrated in HR-TEM images in Fig. 2B, it was clearly observed that all perovskite fibers were made up of spherical nanoparticles with a average size of approximately 30, 50, and 80 nm in diameter for $LaCr_{0.8}Ru_{0.2}O_3$, $LaCr_{0.8}Ru_{0.1}Ni_{0.1}O_3$, and $LaCr_{0.8}Ni_{0.2}O_3$, respectively, which are networked each other to form the hollow fibrous structure. Furthermore, the HR-TEM analysis provides strong evidence for the formation of the micro-tubular feature from the wall with a thickness of over 50 nm at the end of highly interconnected nanoparticles as the dark contrast. Both features provided a large specific surface area of 14.26, 13.65, and 12.33 m^2/g for $LaCr_{0.8}Ru_{0.2}O_3$, $LaCr_{0.8}Ru_{0.1}Ni_{0.1}O_3$, and $LaCr_{0.8}Ni_{0.2}O_3$, respectively, which are ~3 times larger than that of grain nanoparticles prepared in the absence of the ACF template (4.39 m^2/g with a size of ≈50 nm in Fig. S1 and Table S3). It is likely that these hollow fibrous morphology comprising of nanosized particles and their large surface area would provide a short distance of mass transfer for the hydrocarbons in and desired H_2 out easily, resulting in an excellent catalytic performance in the process of oil reforming. As presented in right panel of HR-TEM images, the selected area electron diffraction (SAED) spot patterns for all perovskite hollow fibers were assigned to the [010] and [001] planes along the [100] direction. As shown in the left panel of magnified HR-TEM images, the interplanar distances of $LaCr_{0.8}Ru_{0.2}O_3$, $LaCr_{0.8}Ru_{0.1}Ni_{0.1}O_3$, and $LaCr_{0.8}Ni_{0.2}O_3$ were observed as 0.277, 0.275, and 0.273 nm, respectively, from the regular lattice fringes along the [112] direction. These results are well consistent with the values estimated from the XRD patterns.

To investigate the chemical bonding nature of the Ru/Ni substituted perovskites, the x-ray photoelectron spectroscopy (XPS) peaks corresponding to La 3d, Cr 2p, O 1s, Ru $3p_{3/2}$,and Ni $3p_{3/2}$ of the hollow fibers are displayed in Fig. 3. Binding energies and atomic ratios are determined from the peak fittings are summarized in Table S4 and S5. The two typical peaks of La $3d_{3/2}$ and La $3d_{5/2}$ are observed in Fig. 3A, close to those expected for a La^{3+} ion in an oxide environment. No significant differences were observed in the La $3d_{5/2}$ doublets (La_2O_3 at 838.4 eV and $La(OH)_3$ at 833.9 eV) for the perovskite hollow fibers[28]. For the Cr peaks shown in Fig. 3B, the Cr $2p_{3/2}$ zone was deconvoluted into two valence states: low-valence, Cr^{3+}, at ca. 576.1 eV and high-valence, Cr^{5+} or Cr^{6+}, at ca. 577.6 or 579.2 eV, respectively[30]. Referring to the Ru and Ni substituted perovskite hollow fibers, the Cr $2p_{3/2}$ peaks was more shifted toward higher valence state along with relatively higher proportion of Cr^{5+} or Cr^{6+} than $LaCrO_3$ hollow fiber indicating a sharing of electron density between the Ru/Ni and less electronegative Cr when no significant changes in peak shape was involved. The O 1s spectra shown in Fig. 3C were also split into two peaks: lattice oxygen (O^{2-}) at the lower binding energy (529.4 eV) and surface adsorbed oxygen (O^-) at the higher binding energy (531.2 eV)[30,31]. Considering the higher proportion of adsorbed oxygen on surface for the metal substituted $LaCrO_3$, the spectra were used to estimate the ratio of $O_{surface}/O_{lattice}$ for each hollow fiber, with values of 1.24, 1.57, 1.00 and 0.56 for the $LaCr_{0.8}Ru_{0.2}O_3$, $LaCr_{0.8}Ru_{0.1}Ni_{0.1}O_3$, $LaCr_{0.8}Ni_{0.2}O_3$, $LaCrO_3$, respectively. The higher proportion of surface oxygen of the Ru/Ni substituted hollow fibers compared to the $LaCrO_3$ was likely due to the deformation of the perovskite structure by the metal substitution, which is expected to enhance the catalytic activity at the reaction. In Fig. 3D, the Ru $3p_{3/2}$ peaks (463.9–464.2 eV and 466.8–467.3 eV) of the $LaCr_{0.8}Ru_{0.2}O_3$ and $LaCr_{0.8}Ru_{0.1}Ni_{0.1}O_3$ hollow fibers showed a higher binding energy of $Ru^{High\text{-}Valence}$, formally in the $Ru^{4+/5+}$ mixed-valence states, in the BO_3 inner lattice rather than the outer crystal surface[28,35]. In Fig. 3E, the Ni $3p_{3/2}$ peaks (66.9–68.5 eV and 71.8–74.5 eV) are also shifted to the higher binding energy of $Ni^{High\text{-}Valence}$[29,36]. From these results, the prepared perovskites with metal substitution of Cr^{3+}, Ru^{3+}, or Ni^{3+} are enriched with high-valence of metal cations along with O^- species. These are related to the oxygen surface storage capacity which demonstrates the prevalent role of the Ru, Ni, and Cr redox cycles on the catalytic activity.

The temperature-programmed reductions of H_2 (H_2-TPR) of the perovskite structures are displayed in Fig. 4A. As has been previously reported, the position of the reduction peaks can be affected by crystallite size, oxygen defects, bonding strength, transition metal state/location and doping level of the perovskites[28,30]. The profile from the $LaCr_{0.8}Ru_{0.2}O_3$ hollow fiber showed a two-step consecutive reduction with H_2 consumption peaks at around 325°C and 625°C

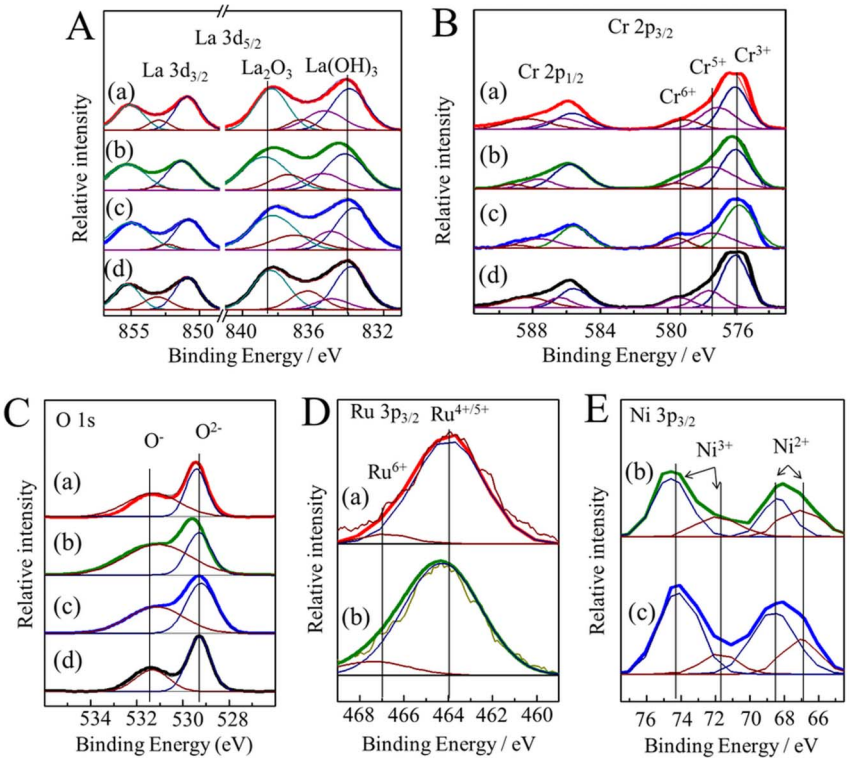

Figure 3 | **XPS spectra of A. La 3d, B. Cr $2p_{3/2}$, C. O 1s, D. Ru $3p_{3/2}$, and E. Ni $3p_{3/2}$ of the hollow fibers: (a) $LaCr_{0.8}Ru_{0.2}O_3$, (b) $LaCr_{0.8}Ru_{0.1}Ni_{0.1}O_3$, (c) $LaCr_{0.8}Ni_{0.2}O_3$, and (d) $LaCrO_3$.**

while two different H_2 consumption peaks was revealed at around 434°C and 516°C for the $LaCr_{0.8}Ni_{0.2}O_3$ hollow fiber. The low-temperature peak is likely to include the reduction of Ru or Ni and Cr ions on the surface, changing them from an oxidized to a lower valance state, while the reduction peak at the higher temperature can be attributed to the further reduction of Ru or Ni and Cr ions in the perovskites framework. The first reduction peak of $LaCr_{0.8}Ru_{0.2}O_3$ was observed to shift to a lower temperature on partial substitution of Cr by Ru in the B site of the $LaCrO_3$ structure. In case of the $LaCr_{0.8}Ru_{0.1}Ni_{0.1}O_3$ hollow fiber showed small peak shifted to the lower temperature of 222 °C at first reduction than $LaCr_{0.8}Ru_{0.2}O_3$ hollow fiber; this may be due to the outer-lattice Ru/Ni metals rather than inner-lattice Ru/Ni oxides. Compared to the other perovskites, the highest reduction peak for the $LaCr_{0.8}Ru_{0.2}O_3$ hollow fiber appeared with a greater peak area at the relatively higher temperature which can be inferred to the presence of a higher quantity of Ru incorporation into the lattice, along with the $Cr^{High\text{-}Valence}$ species that are strongly bonded to O[30]. The profile of $LaCr_{0.8}Ru_{0.2}O_3$ hollow fiber indicated then an improved reducibility with higher amount of H_2 consumption and material structural stability from TPR profiles, which is accessible to ATR reaction.

It should be noted that the ACF template used in the preparation of the perovskite hollow fibers can act as a combustible agent when hot spots due to burning of the carbon could be responsible for higher actual temperatures to induce mixed valance states that would enhance the mobility of oxygen in the lattice[25–27]. As is well known, when hydrocarbon species adsorb along with the O atoms, electrons transfer from the active metals neighbouring the vacancy at the B site to the reactants, facilitating cleavage of the C–H bond to release H_2. It is, therefore, expected that the hollow fiber with a high percentage of $Ru^{High\text{-}Valence}$, $Ni^{High\text{-}Valence}$, $Cr^{High\text{-}Valence}$, and O^- species correlated to partial incorporation of Ru/Ni is superior in the redox catalysis in the reforming of hydrocarbon fuels to H_2 gas.

Discussion

In a preliminary study as plotted in Fig. 4B and Fig. S2, the effects of the fibrous structure and Ru/Ni substitution in the catalyst activity were investigated: H_2 production from heavy hydrocarbon, hexadecane ($C_{16}H_{34}$), with an addition of sulphur, Dibenzothiophene, at content of 100 ppm. All tested catalysts had conversions of the liquid hexadecane over 99% at the conditions of 1027 K, molar ratio of $H_2O/O_2/C = 1.25/0.4/1$ and GHSV of 4000 h^{-1}. For a comparison with the hollow fiber catalyst, the grain powder catalyst was prepared by using the similar method without ACF template as a reference. Notably, the hollow fibers show not only a superior reforming activity but also a better durability on the H_2 production than the grain powder without any drop of performance during 50 hr operation. As displayed in Fig. 4B(a)–4B(g), the $LaCr_{0.8}Ru_{0.1}Ni_{0.1}O_3$ and $LaCr_{0.8}Ru_{0.2}O_3$ hollow fibers exhibited about 1.5 fold improvements in the H_2 production activity than those corresponding grain powders. This result is due to the better mass/heat transfer of the tubular architecture through ACF template during the autothermal reforming process as well as more structural oxidation by combustion effect of the ACF.

The $LaCr_{0.8}Ru_{0.2}O_3$ hollow fiber achieved a high initial H_2 production of 66 mol% (H_2 mol%) including no degradation in the performance for 50 hr with CO_x selectivity values of nearly 90% due to the active phase and stable structure in the redox catalysis reaction proved from the characterization data. Furthermore, the $LaCr_{0.8}Ni_{0.2}O_3$ and $LaCr_{0.8}Ru_{0.1}Ni_{0.1}O_3$ fibers demonstrated a very high level of the production of H_2, 71 mol% and 73 mol%, respectively. For 50 hr reaction, sustainable H_2 production activities are observed in both Ru-substituted hollow fibers (Fig. 4B(a) and 4B(b)). Only Ni-substituted hollow fiber suffered in regards to durability for the long-term reaction because nickel-contained catalysts have generally shown catalyst deactivation by heavy carbon deposition (i.e. coke) on the catalyst surface[37]. This can be confirmed by large deposited carbon amount on the catalyst surfaces based on the TGA data (Fig. S3). As for comparison with the conventional 5%

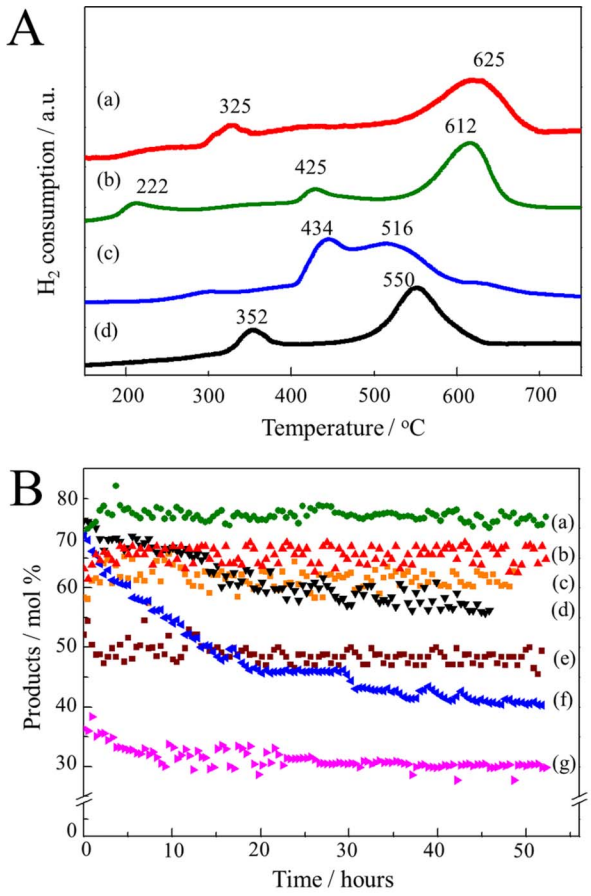

Figure 4 | A. H_2–TPR profiles of the hollow fibers: (a) $LaCr_{0.8}Ru_{0.2}O_3$, (b) $LaCr_{0.8}Ru_{0.1}Ni_{0.1}O_3$, (c) $LaCr_{0.8}Ni_{0.2}O_3$, and (d) $LaCrO_3$. B. H_2 production (mol%) of as-prepared perovkskite catalysts for ATR reaction using hexadecane ($C_{16}H_{34}$), with an addition of sulphur, Dibenzothiophene, at content of 100 ppm: (a) $LaCr_{0.8}Ru_{0.1}Ni_{0.1}O_3$ hollow fiber, (b) $LaCr_{0.8}Ru_{0.2}O_3$ hollow fiber, (c) $LaCr_{0.8}Ru_{0.1}Ni_{0.1}O_3$ grain, (d) Pt-GDC, (e) $LaCr_{0.8}Ru_{0.2}O_3$ grain, (f) $LaCr_{0.8}Ni_{0.2}O_3$ hollow fiber, and (g) $LaCrO_3$ hollow fiber. ($C_{16}H_{34}$ = 0.012 ml·min^{-1}, $H_2O/O_2/C$ = 1.25/0.4/1, 1027 K, GHSV = 4000 h^{-1}).

Pt-gadolinium-doped CeO_2 (GDC) which is considered as a noble catalyst prepared by incipient wetness impregnation, there was also a remarkable drop of the H_2 production efficiency under sulphur (100 ppm) contained hydrocarbon in spite of the similar initial performance. It can be understood as sulphur poisoning on the Pt metal surface being the active site for the large coke deposition (Fig. S3) whereas great sulphur endurance was revealed at the $LaCr_{0.8}Ru_{0.2}O_3$ catalyst. As a result, it was found that the $LaCr_{0.8}Ru_{0.2}O_3$ hollow fiber in particular, was seen to be highly effective in converting the surrogate fuel to H_2-rich reformates and much more stable than the other perovskites.

For the first try of the gas oil reforming, gas oils obtained from Arabian light oil (LGO), medium oil (MGO), heavy oil (HGO), and diesel were subjected to detailed analysis to assess levels of reactive and refractory S, N, and C species, using GC coupled with an atomic emission detector (GC–AED), as illustrated in Figs. 5A–5C and summarized the amount of each species in Table 1. Refractory S and alkylcarbazole (C_x-Cz) contents were significantly (3–4 times) higher for the HGO than the LGO. Although the boiling point ranges of the gas oils were same (220–340°C), the distribution of C species varied between the samples, as is evident in the GC–AED chromatographs[7–9]. HGO contained almost no species less than C_{12} and had high amounts of C_{18}–C_{20}. The diesel exhibited a similar C profile to LGO, with much smaller molecules evident. The distribution of S species in the gas oil was significantly different. The major S species were alkyl-benzothiophenes (Alkyl-BTs) comprising C_2–C_5 alkyl chains, dibenzothiophene (DBT), and considerable amounts of alkyl-DBTs. HGO contained the largest amount of alkyl-DBTs with two or more alkyl C atoms, which are classed as the refractory S species[8]. The GC–AED chromatographs of N species, presented in Fig. 4C, clearly indicate a significantly higher N content in HGO, which is mainly due to C_x–Cz[9]. The concentrations of S and N for commercial diesel were found to be negligible compared to the gas oils.

The time dependance of ATR experiments involving the three different gas oils, as well as the commercial diesel, were subsequently conducted over the Pt–GDC and the as-prepared $LaCr_{0.8}Ru_{0.2}O_3$ catalysts, as shown in Figs. 5D, 5E, S4, and S5. The product distributions from S- and N-free diesel reforming are shown in Figs. 5D and S4. H_2 production by the hollow fiber was continuously stable at 53 mol% over the time period tested, and there was no evidence of catalyst deactivation. The loss in catalytic activity of the Pt–GDC (from 50 to 37 mol%) while reforming the diesel may be partially attributed to the presence of coke from unreacted polyaromatics in the fuel.

Fig. 5E show the H_2 produced when the gas oils were homogeneously fed in the presence of high quantities of S and N (up to 17,000 ppm and 312 ppm, respectively). It was found that excellent hydrogen production, together with the tolerance of S and N compounds on the feeds could be achieved over perovskite hollow fiber comparing to conventional Pt–GDC. For the long periods of time-on-stream (~50 h), the H_2 production by the hollow fiber, averaged from the steady state, achieved almost 47.4 mol% for LGO, 39.3 mol% for MGO, and 34.6 mol% for HGO (Fig. 5E). H_2 production from HGO varied significantly depending on the catalyst, with average values of 34.6 mol%, 23.3 mol%, and 7.7 mol% for the $LaCr_{0.8}Ru_{0.2}O_3$ hollow fiber, $LaCr_{0.8}Ru_{0.2}O_3$ grains, and Pt–GDC, respectively, with a decrease in the order: $LaCr_{0.8}Ru_{0.2}O_3$ hollow fiber > $LaCr_{0.8}Ru_{0.2}O_3$ grain > Pt–GDC. In addition, the higher reforming capacity of the $LaCr_{0.8}Ru_{0.2}O_3$ hollow fiber was reflected in the lower proportion of non-reformed hydrocarbons (CH_4, C_2H_4, C_2H_6, and C_3H_6) in the products, as displayed in Fig. S5. The increase in H_2 was also accompanied by a decrease in CO_x for all of the tested catalysts. As expected, it was observed that the $LaCr_{0.8}Ru_{0.2}O_3$ hollow fiber material exhibited higher activity and increased stability with a lower degree of deactivation, whereas the perovskite grain and the Pt–GDC were substantially deactivated over the reaction time period. This loss in ATR activity can be attributed to S poisoning and coke formation on the catalytic surface. As can be seen in Table 2, the quantity of C and S residues deposited on each used catalyst correlated with the concentrations of S, N, and aromatic species contained in the gas oil fuels. After long-term reaction, even in HGO, the decrease in the deposited quantities of S and C were close to 80%, 61% and 52% for the hollow fiber, grain and Pt–GDC, respectively. This better tolerance under severe gas oil is in accordance with the higher reforming efficiency and stability observed for the $LaCr_{0.8}Ru_{0.2}O_3$ hollow fiber, which is strongly associated with the improved mass/heat transfer rates by the microtubular structure with higher effective surface area and reactivity owing to the well incorporation of Ru in the perovskite lattice.

The durable stability of perovskite catalysts is important issue for their practical industry applications. The reforming process using HGO was repeated four times, as shown in Fig. 5F. When reforming process using HGO was repeated for each cycle, the used $LaCr_{0.8}Ru_{0.2}O_3$ hollow fiber was routinely refreshed by combusting under air atmosphere at 1027 K to remove carbonaceous deposits (coke) and supplied to the reactor. The same quantities of products were constantly achieved for each 24 h cycle, which may be due to the sustainable hollow fibrous architecture composed of $LaCr_{0.8}Ru_{0.2}O_3$ nanoparticles networks along with slight sintering and stable structure without any reduction or segregation of the metals as from the SEM and XRD analysis in Fig. 5G.

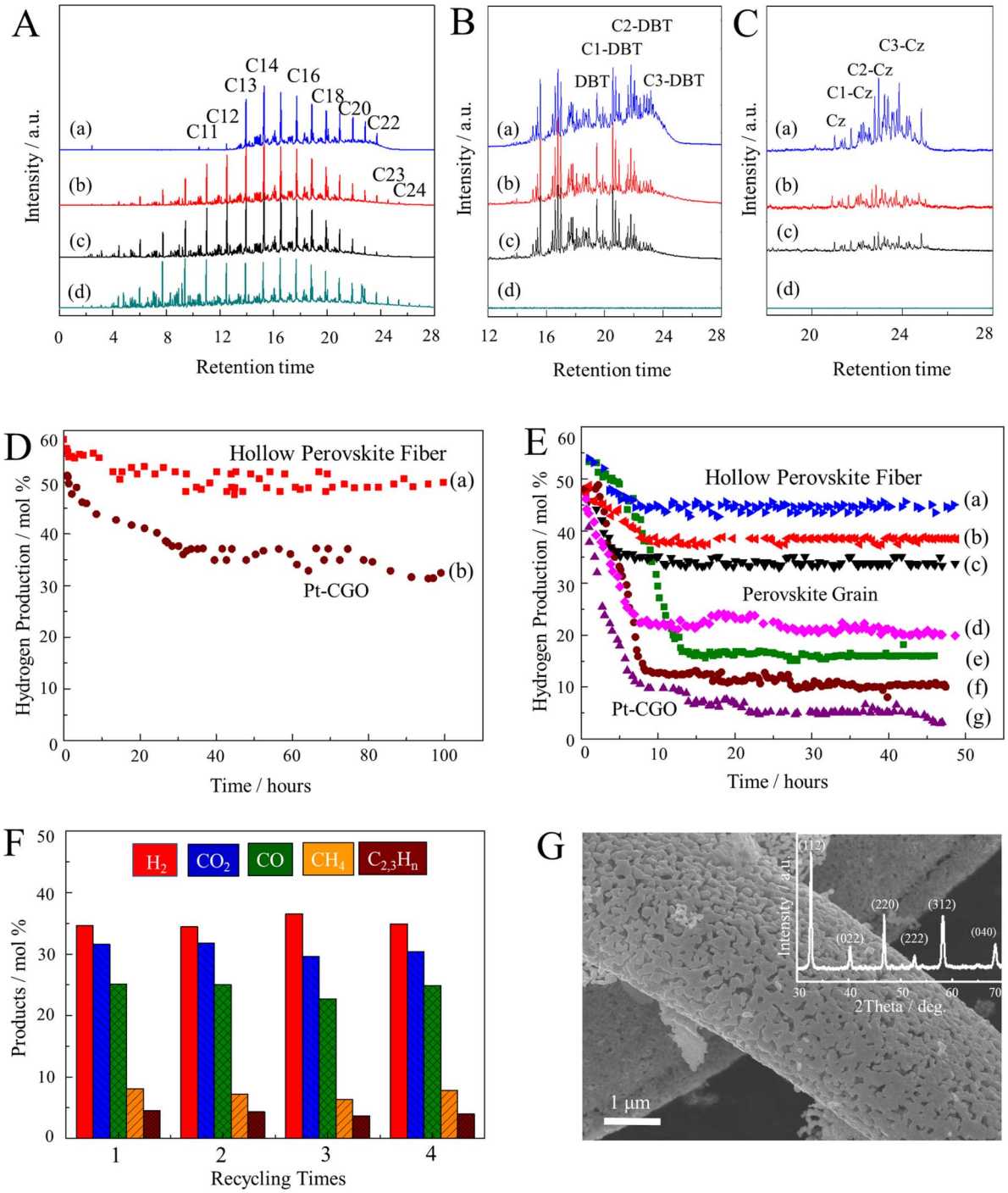

Figure 5 | GC–AED profiles for A. carbon, B. sulfur, and C. nitrogen species of the (a) HGO, (b), MGO (c) LGO, and (d) diesel. D. H_2 production for diesel of the (a) $LaCr_{0.8}Ru_{0.2}O_3$ hollow fiber and (b) Pt–GDC. E. H_2 production of the (a) LGO ($LaCr_{0.8}Ru_{0.2}O_3$ hollow fiber), (b) MGO ($LaCr_{0.8}Ru_{0.2}O_3$ hollow fiber), (c) HGO ($LaCr_{0.8}Ru_{0.2}O_3$ hollow fiber), (d) HGO ($LaCr_{0.8}Ru_{0.2}O_3$ grain), (e) LGO (Pt–GDC), (f) MGO (Pt–GDC), and (g) HGO (Pt–GDC). F. Recycling test of the $LaCr_{0.8}Ru_{0.2}O_3$ hollow fiber using HGO. (all fuels = 0.012 ml·min^{-1}, $H_2O/O_2/C$ = 1.25 : 0.4 : 1, 1027 K, GHSV = 4000 h^{-1}). G. SEM image and XRD patterns (inset) of the $LaCr_{0.8}Ru_{0.2}O_3$ hollow fiber refreshed after HGO reforming.

Table 1 | Composition of (a) LGO, (b) MGO, and (c) HGO

	Total Aromatics (%)	Sulfur (ppm)		Nitrogen (ppm)	
		Reactive	Refractory	Cz	Alkyl-Cz
(a)	21	4,133.5	3,566.5	1.4	83.6
(b)	25	4,741.4	5,858.6	3.1	94.9
(c)	32	6,500.0	10,500.0	4.3	307.7

In conclusion, we demonstrated the synthesis of the hollow fiber networked with perovskite nanoparticles of $LaCr_{0.8}Ru_{0.2}O_3$, $LaCr_{0.8}Ru_{0.1}Ni_{0.1}O_3$, and $LaCr_{0.8}Ni_{0.2}O_3$ using ACF as a sacrificial template for heavy oil reforming. The hollow fiber had a well-crystallized structure and a high specific surface area of ≈13 m^2/g was revealed with an average particle size of ≈50 nm, which is ~3 times larger than that of grains. The $LaCr_{0.8}Ru_{0.2}O_3$ hollow fibrous architecture had a favorable effect on the capacity to yield H_2 directly from heavy gas oil reforming, at 34.6 mol% compared to grain (23.3

Table 2 | Elemental analysis by CHNS after ATR of the (a) LGO ($LaCr_{0.8}Ru_{0.2}O_3$ hollow fiber), (b) MGO ($LaCr_{0.8}Ru_{0.2}O_3$ hollow fiber), (c) HGO ($LaCr_{0.8}Ru_{0.2}O_3$ hollow fiber), (d) HGO ($LaCr_{0.8}Ru_{0.2}O_3$ grain), (e) LGO (Pt–GDC), (f) MGO (Pt–GDC), and (g) HGO (Pt–GDC)

	Content (wt%)						
	(a)	(b)	(c)	(d)	(e)	(f)	(g)
Carbon	11.52	15.75	18.77	25.47	34.05	35.30	39.15
Sulfur	0.03	0.14	0.17	0.21	0.40	0.78	0.99

mol%) and Pt–GDC (7.7 mol%), with substantial durability even for long-term reactions with high concentrations of S, N, and aromatic compounds.

Methods

Synthesis of perovskite hollow fibers of $LaCrAO_3$ (A = Ru and/or Ni). Perovskite hollow fibers were prepared by using aqueous (solution) impregnation synthesis which is a rapid and convenient method to provide high surface area oxides. An ACF template (1 g) was serially treated with H_2SO_4 (6 M) and HNO_3 (6 M) and then soaked in a mixed aqueous solution of $La(NO_3)_3{\cdot}9H_2O$ (0.15 M), $Cr(NO_3)_3{\cdot}9H_2O$ (0.1 M), Ni(NO3)2·9H_2O (0.01 M or 0.02 M),and $HN_4O_{10}Ru$ (0.01 M or 0.02 M) for 24 hours. After washing with deionized water, the ACF impregnated with La^{III}/$Cr^{III}_{0.8}$/(Ru^{III} and/or Ni^{II}) ions was then calcined at 1027 K for 6 h in sufficient air flow to form perovskite hollow fibers. For comparison, $LaCr_{0.8}Ru_{0.2}O_3$ grain was prepared in the absence of the ACF under the same conditions. The 5% Pt–GDC (gadolinium-doped CeO_2) was prepared by incipient wetness impregnation in a similar manner[6].

Analyses of the commercial diesel and gas oils. Three different fuels were selected: hexadecane (Sigma–Aldrich) containing 100 ppm of sulphur (Dibenzothiophene, Sigma–Aldrich), commercial diesel (GS Caltex Co. Korea), and gas oils to investigate the reforming performances of the test catalysts. Gas oils were produced from the light (LGO), medium (MGO) and heavy (HGO) Saudi Arabian crude oils. Commercial diesel was collected from GS Caltex Co. Korea. Carbon, sulfur, nitrogen species of all fuels were monitored by gas chromatography (GC, HP6890) equipped with an atomic emission detector (AED, G2350A) at conditions summarized in Table S6. High performance liquid chromatography (HPLC) technique was applied for determination of aromatic components using Hitachi L-6200 unit equipped with D-700 DAD detector (λ = 254 nm). A 0.46 cm × 25 cm column, packed with 5 μm Zorbax-ODS, was used at 25°C. Mobile phase was a mixture of methanol and water (85 : 15 vol/vol) with the flow rate of 1.0 ml/min.

H_2 Production test. The autothermal reforming of gas oil fuels was carried out at atmospheric pressure in a fixed-bed stainless steel flow reactor with 8 mm internal diameter. The temperature of the reactor was monitored and controlled by thermocouples that were coaxially inserted into the center of the catalyst bed. The fuels were injected by liquid pump and ultrasonic injector for homogeneous fuel supply. For ATR experiments of the hollow fiber catalysts, each feed, with a molar ratio of $H_2O/O_2/C$ = 1.25 : 0.4 : 1, was introduced into the reactor by a mass flow controller (flow rate = 0.012 ml·min^{-1} and GHSV = 4000 h^{-1}), where the reforming reaction of each hollow fiber catalyst (0.5 g) was carried out for 50–100 h at 1027 K at atmospheric pressure. All reformates (H_2, CO_2, CO, CH_4, $C_{2,3}H_n$) were periodically measured using on-line GC (Youglin-6000) equipped with a TC detector and an FI detector which were programmed to operate under high-sensitivity conditions, and the product distributions were averaged from the steady state. The conversion and hydrogen mole percentage of products by hexadecane, diesel and gas oils are defined as follows:

- Fuel conversions at the liquid base were over 99%.
- Product distribution: (%) (i: H_2, CO, CH_4, CO_2, $C_{2,3}H_n$ (C_2H_4 + C_2H_6 + C_3H_6)):

$$\frac{(mole\quad i)_{out}}{\sum mole\quad i_{out}} \times 100$$

1. Yu, K. *et al.* Non-syngas direct steam reforming of methanol to hydrogen and carbon dioxide at low temperature. *Nat. Commun.* **3**, 1230 (2012).
2. Choudhary, T. V. & Choudhary, V. R. Energy-Efficient Syngas Production through Catalytic Oxy-Methane Reforming Reactions. *Angew. Chem. Int. Ed.* **47**, 1828–1847 (2008).
3. Deluga, G. A., Salge, J. R., Schmidt, L. D. & Verykios, X. E. Renewable hydrogen from ethanol by autothermal reforming. *Science* **303**, 993–997 (2004).
4. Baudouin, D. *et al.* Nickel–Silicide Colloid Prepared under Mild Conditions as a Versatile Ni Precursor for More Efficient CO_2 Reforming of CH_4 Catalysts. *J. Am. Chem. Soc.* **134**, 20624–20627 (2012).
5. Navarro, R. M. *et al.* Catalysts for Hydrogen Production from Heavy Hydrocarbons. *ChemCatChem* **3**, 440–457 (2011).
6. Kang, I., Bae, J. M. & Bae, G. J. Performance comparison of autothermal reforming for liquid hydrocarbons, gasoline and diesel for fuel cell applications. *J. Power Sources* **163**, 538–546 (2006).
7. Park, J. I. *et al.* Characteristics on HDS over amorphous silica-alumina in single and dual catalytic bed system for gas oil. *Catal. Today* **164**, 100–106 (2011).
8. Kim, T. G. *et al.* Analysis and deep hydrodesulfurization reactivity of Saudi Arabian gas oils. *J. Ind. Eng. Chem.* in press (2013).
9. Murti, S. D. S., Yang, H., Choi, K. H., Korai, Y. & Mochida, I. Influences of nitrogen species on the hydrodesulfurization reactivity of a gas oil over sulfide catalysts of variable activity. *Appl. Catal. A-Gen.* **252**, 331–346 (2003).
10. Chen, Y., Xie, C., Li, Y., Song, C. & Bolin, T. B. Sulfur poisoning mechanism of steam reforming catalysts: an X-ray absorption near edge structure (XANES) spectroscopic study. *Phys. Chem. Chem. Phys.* **12**, 5707–5711 (2010).
11. Xie, C., Chen, Y., Engelhard, M. H. & Song, C. Comparative Study on the Sulfur Tolerance and Carbon Resistance of Supported Noble Metal Catalysts in Steam Reforming of Liquid Hydrocarbon Fuel. *ACS Catal.* **2**, 1127–1137 (2012).
12. Nikolla, E., Holewinski, A., Schwank, J. & Linic, S. Controlling Carbon Surface Chemistry by Alloying: Carbon Tolerant Reforming Catalyst. *J. Am. Chem. Soc.* **128**, 11354–11355 (2006).
13. Pena, M. A. & Fierro, J. L. G. Chemical Structures and Performance of Perovskite Oxides. *Chem. Rev.* **101**, 1981–2017 (2001).
14. Suntivich, J. *et al.* Design principles for oxygen-reduction activity on perovskite oxide catalysts for fuel cells and metal–air batteries. *Nat. Chem.* **3**, 546–550 (2011).
15. Ogawa, M. & Kuroda, K. Photofunctions of Intercalation Compounds. *Chem. Rev.* **95**, 399–438 (1995).
16. Ida, S. *et al.* Photoluminescence of Perovskite Nanosheets Prepared by Exfoliation of Layered Oxides, $K_2Ln_2Ti_3O_{10}$, $KLnNb_2O_7$, and $RbLnTa_2O_7$ (Ln: Lanthanide Ion). *J. Am. Chem. Soc.* **130**, 7052–7059 (2008).
17. Jin, H., Rhim, S. H., Im, J. & Freeman, A. J. Topological Oxide Insulator in Cubic Perovskite Structure. *Sci. Rep.* **3**, 1651 (2013).
18. Meyers, D. *et al.* Zhang-Rice physics and anomalous copper states in A-site ordered perovskites. *Sci. Rep.* **3**, 1834 (2013).
19. Zhou, H. *et al.* Leaf-architectured 3D Hierarchical Artificial Photosynthetic System of Perovskite Titanates towards CO_2 Photoreduction into Hydrocarbon Fuels. *Sci. Rep.* **3**, 1667 (2013).
20. Ball, J. M., Lee, M., Heya, A. & Snaith, H. J. Low-temperature processed meso-superstructured to thin-film perovskite solar cells. *Energy Environ. Sci.* **6**, 1739–1743 (2013).
21. Dong, D. *et al.* Eggshell membrane-templated synthesis of highly crystalline perovskite ceramics for solid oxide fuel cells. *J. Mater. Chem.* **21**, 1028–1032 (2011).
22. Park, D. H., Kim, J. E., Oh, J. M., Shul, Y. G. & Choy, J. H. DNA Core@Inorganic Shell. *J. Am. Chem. Soc.* **132**, 16753–16753 (2010).
23. Li, S. *et al.* Soot trapping and combustion on nanofibrous perovskite $LaMnO_3$ catalysts under a continuous flow of soot. *Appl. Catal. B-Environ.* **93**, 383–386 (2010).
24. Nuraje, N. *et al.* Biotemplated Synthesis of Perovskite Nanomaterials for Solar Energy Conversion. *Adv. Mater.* **24**, 2885 (2012).
25. Blanco, J. *et al.* Novel One-Step Synthesis of Porous-Supported Catalysts by Activated-Carbon Templating. *Adv. Mater.* **18**, 1162–1165 (2006).
26. Civera, A., Pavese, M., Saracco, G. & Specchia, V. Combustion synthesis of perovskite-type catalysts for natural gas combustion. *Catal. Today* **83**, 199–211 (2003).
27. Kim, H. J., Nam, K. H. & Shul, Y. G. Preparation of TiO_2 fiber and its photocatalytic properties. *Mater. Sci. Forum* **439**, 271–276 (2003).
28. Mota, N. *et al.* Insights on the role of Ru substitution in the properties of $LaCoO_3$-based oxides as catalysts precursors for the oxidative reforming of diesel fuel. *Appl. Catal. B-Environ.* **113–114**, 271–280 (2012).
29. Mawdsley, J. R., Vaughey, J. T. & Krause, T. R. Neutron Diffraction Studies of Nickel-Containing Perovskite Oxide Catalysts Exposed to Autothermal Reforming Environments. *Chem. Mater.* **21**, 4830–4838 (2009).
30. Rida, K. *et al.* Effect of calcination temperature on the structural characteristics and catalytic activity for propene combustion of sol–gel derived lanthanum chromite perovskite. *Appl. Catal. A-Gen.* **327**, 173–179 (2007).
31. Fino, D., Russo, N., Cauda, E., Saracco, G. & Specchia, V. La–Li–Cr perovskite catalysts for diesel particulate combustion. *Catal. Today* **114**, 31–39 (2006).
32. Matatov-Meytal, Y. & Sheintuch, M. Catalytic fibers and cloths. *Appl. Catal. A-Gen.* **231**, 1–16 (2002).
33. Sunarso, J., Torriero, A. J., Zhou, W., Howlett, P. C. & Forsyth, M. Oxygen Reduction Reaction Activity of La-Based Perovskite Oxides in Alkaline Medium: A Thin-Film Rotating Ring-Disk Electrode Study. *J. Phys. Chem. C* **116**, 5827–5834 (2012).
34. Shannon, R. D. Revised effective ionic radii and systematic studies of interatomic distances in halides and chalcogenides. *Acta Cryst.* **A32**, 751–767 (1976).
35. Gaur, S., Pakhare, D., Wu, H., Haynes, D. J. & Spivey, J. J. CO_2 Reforming of CH_4 over Ru-Substituted Pyrochlore Catalysts: Effects of Temperature and Reactant Feed Ratio. *Energ. Fuel.* **26**, 1989–1998 (2012).

36. Qiao, L. & Bi, X. Direct observation of Ni^{3+} and Ni^{2+} in correlated $LaNiO_{3-\delta}$ films. *EPL* **93**, 57002p1–57002p6 (2011).
37. Ertl, G., Knozinger, H. & Weitkamp, J. Handbook of Heterogeneous Catalysis, Wiley VCH, Weinheim (1997).

Acknowledgments

This work was supported by a National Research Foundation of Korea (NRF) grant funded by the Korea government (MEST) (No. 2009-C1AAA001-2009-0092926 and No. 2012R1A2A2A02011268), and we thank GS Caltex Corporation for partial support.

Author contributions

Y.K.J., D.H.P. and J.I.P. carried out the experiments, analyzed the data, and wrote the manuscript. S.H.Y., I.M. and J.H.C. contributed to critical discussions on gas oil analyses and material characterizations. Y.G.S. and J. I. P. conceived the original idea, designed and supervised the whole study, and made critical comments on the manuscript. All authors reviewed the manuscript.

Additional information

Supplementary information accompanies this paper at http://www.nature.com/scientificreports

Competing financial interests: The authors declare no competing financial interests.

How to cite this article: Jeon, Y. *et al.* Hollow Fibers Networked with Perovskite Nanoparticles for H_2 Production from Heavy Oil. *Sci. Rep.* **3**, 2902; DOI:10.1038/srep02902 (2013).